Past and future discharge and stream temperature at high spatial resolution in a large European basin (Loire basin, France)

Hanieh Seyedhashemi[1,2], Florentina Moatar[1], Jean-Philippe Vidal[1], and Dominique Thiéry[3]

[1]INRAE, UR RiverLy, 5 rue de la Doua CS 20244, 69625 Villeurbanne, France
[2]EA 6293 GéoHydrosystèmes COntinentaux, Université François-Rabelais de Tours, Parc de Grandmont, 37200 Tours, France
[3]BRGM, Bureau de Recherches Géologiques et Minières, BP 6009 45060 Orléans Cedex 2, France
Correspondence: Hanieh Seyedhashemi (hanieh.seyedhashemi@inrae.fr)

Abstract.

This paper presents retrospective simulations (1963-2019) and future projections (1976-2100) of daily time series of discharge and stream temperature for 52 278 reaches (median length=1.3 km) over the Loire River basin (10^5 km^2) in France, using a physical process-based thermal model coupled with a semi-distributed hydrological model. Retrospective simulations

5 ~~over the 1963–2019~~ are based on the 8 km gridded Safran meteorological reanalysis over France. 21st century projections are based on a subset of the ~~DRIAS2020 ensemble projection dataset , derived from the Euro Cordex data set through the ADAMONT statistical bias correction. Such a dataset at this~~ 8 km gridded and bias-corrected DRIAS-2020 dataset over France. The discharge and stream temperature dataset stands out from existing ones thanks to its large scale and its high spatial resolution~~stands out from existing datasets, and is the first one in France derived from~~, and the use of a physical process-based

10 thermal model. The whole dataset is freely available ~~for other studies~~ and can be downloaded ~~as~~ in NetCDF format from ~~https://doi.org/10.57745/LBPGFS~~ https://doi.org/10.57745/LBPGFS (Seyedhashemi et al., 2022a).

1   Introduction

Stream (water) temperature (Tw) is a critical parameter affecting the eutrophication of water bodies (Minaudo et al., 2018; Le Moal et al., 2019; Zhao et al., 2022), a wide range of biogeochemical processes (Ouellet et al., 2020), the life cycle (Elliott

15 and Elliott, 2010) and spatial distribution of aquatic organisms (Cox and Rutherford, 2000; Morales-Marín et al., 2019; Picard et al., 2022). Recent evidence suggests the worldwide rise in this critical parameter due to climate change over the past decades (e.g. Moatar and Gailhard, 2006; Orr et al., 2015; Arora et al., 2016; Michel et al., 2020; Seyedhashemi et al., 2022b), which is also anticipated to continue in the future (e.g. Kwak et al., 2017; Carlson et al., 2017; Seixas et al., 2018; Du et al., 2019; Lee et al., 2020; Piotrowski et al., 2021; Michel et al., 2021). However, missing continuous long-term Tw data at a large scale

20 over the past ~~and future~~ (Nelson and Palmer, 2007; Webb et al., 2008; Arora et al., 2016) has limited our understanding of large-scale controlling factors and spatio-temporal variability of thermal regimes, and of the impacts of such a variability on stream ecosystems in light of climate change (Hannah and Garner, 2015).

To overcome the lack of Tw data and to understand how the thermal regime respond to the climate change, physically-based, or deterministic, models can be used (Dugdale et al., 2017). These models simulate and project Tw dynamics through a heat budget, accounting for energy exchanges and effects of landscape characteristics on energy transfer (Sinokrot et al., 1995; Webb and Walling, 1997; Yearsley, 2009; van Vliet et al., 2013; Beaufort et al., 2016b). Depending on the input data, these models can be run at different temporal resolution and spatial scales, ranging from small streams to large rivers (Dugdale et al., 2017). The outputs of these models allow detecting past and future changes in rivers' thermal regime and exploring the influence of hydroclimatic – i.e. air temperature (Ta) and discharge (Q) – and basin drivers on such changes (see recent studies e.g. Seyedhashemi et al., 2022b; Michel et al., 2021). For example, Seyedhashemi et al. (2022b), using a physical process-based thermal model, found that Tw increased faster than air temperature over the past recent decades, and attributed such an increase in Tw to the increase in Ta and decrease in Q. They also found the greatest increase in large rivers, while riparian shading mitigated the increase in Tw in small mountainuous streams. Additionally, climate-induced changes in Tw could also help us to predict the vulnerability of aquatic species to climate change (Lee et al., 2020).

This paper, using outputs of the 1-D Temperature-NETwork (T-NET) physical process-based thermal model coupled with the EROS semi-distributed hydrological model, presents daily time series of Q and Tw from the past to future at the reach scale over the Loire River basin (10^5 km^2), one of the largest in Europe. ~~Section ?? briefly describes how such a dataset was produced using the above models. Retrospective simulations based on the Safran reanalysis over the 1963–2019 period are then presented in Sec. ??. Future~~ EROS and Q data are presented in section 2. T-NET and Tw data are presented in section 3. Although the time series of both Q and Tw ~~projections derived from the DRIAS2020 climate projection dataset, are then presented in Sec. ??. Note that retrospective simulations have also been commented previously by Seyedhashemi et al. (2022b)~~ are available for the whole year, here, data description is mostly focused on June to August months (hereafter referred to as summer), the time of the year which is crucial for the survival (Steel et al., 2017), growth, and migration of aquatic communities (Arevalo et al., 2020). Note that a part of retrospective simulations has also been previously commented by Seyedhashemi et al. (2022b).

2 ~~Methodology for retrospective simulation~~ EROS hydrological model and ~~projections~~ daily discharge data

2.1 ~~Hydrological~~ Principles and ~~thermal models~~ input data of EROS

~~We use the 1-D Temperature-NETwork (T-NET) physical process-based thermal model coupled with the EROS~~ EROS is a semi-distributed hydrological model ~~to estimate daily Q and Tw for 52 278 reaches (median length=1.3 km) over the Loire River basin in France, one of the largest in Europe (10^5 km^2). The EROS model uses daily air temperature (Ta), precipitation (P) and potential evapotranspiration (PET) to simulate daily streamflow (Q)~~ which simulates daily discharge at the outlet of 368 homogeneous (with respect to land use and geology) sub-basins ~~(see Figure 1, top panel, middle). Then, through a routine in the T-NET model, Q is redistributed along the river network inside~~ for the Loire River basin (see Fig. 1). At the outlet of each sub-basin ~~according to the each reach drainage area. The T-NET model uses these estimated Q, Ta, shortwave net solar radiation (Hns), longwave radiation (Hla), specific humidity (RH), and wind velocity (W) at hourly time step to estimate hourly Tw at each reach by solving the local heat budget, while accounting for thermal propagation and confluence mixing.~~

Finally, hourly outputs of T-NET (Q and Tw) are averaged at the daily scale. Models used here do not consider the influence of water-abstractions and impoundments i.e. simulate natural Q and Tw time series.

Detailed information on models principles, input data, calibration and validation can be found in Thiéry and Moutzopoulos (1995); Thiéry and shortly in Seyedhashemi et al. (2022b) for EROS, and Beaufort et al. (2016a); Loicq et al. (2018); Seyedhashemi et al. (2022b) for T-NET. For both EROS and T-NET, meteorological data (i.e. Ta, P, the water balance is modelled by a lumped model using three reservoirs (see Fig. S2 in the Supplement material of Seyedhashemi et al., 2022b) and a routing function for propagation across sub-basins. To reconstruct daily Q at the sub-basins outlets ("Retrospective simulations" in Fig. 1), EROS uses daily air temperature (Ta, PET, Hns, Hla, RH and W) for retrospective simulations (1963–2019) and projections (1976–2100) come from from different datasets described below. Nevertheless, meterological datasets share the same 8-km grid resolution. All reaches within a grid cell are assigned meteorological data values in that grid cell. For reaches flowing through more than one grid cell, meteorological variables are weighted by the relative length of the reach within each grid cell (Seyedhashemi et al., 2020) . Figure 1 summarises the methodology of reconstruction and projections of daily Q and Tw over the Loire River basin. Figure ?? shows the data availablity for the different simulations.

Synthetic diagram showing the methodology of retrospective simulation and projections of daily Q and Tw over the Loire River basin. The top panel shows the spatial resolution of input data in each step. The red circle points show the outlets of 368 sub-basins. The three black triangle points show the position of sub-basin examples in the southern (L'Allier at Monistrol-d'Allier), middle (L'Arnon at Méreau Pont de Méreau) and northern part (La Loire at Montjean) of the basin used in the text. Solid black lines show the three main Hydro-Ecoregion (HER) delineations in the basin identified by Wasson et al. (2002) through grouping homogeneous areas in terms of land use/land cover, geology, and climate conditions (see Figure 1 of Seyedhashemi et al., .

Period of available daily Q and Tw data for retrospective simulation and projections.

2.2 Retrospective simulation (1963–2019)

To reconstruct daily time series of Q and Tw over the past decades, the meteorological data °C), precipitation (P, mm) and potential evapotranspiration (ET0, mm) computed with the Penman–Monteith equation (Allen et al., 1998). These meteorological data are provided by the 8 km gridded Safran atmospheric reanalysis data (Quintana-Segui et al., 2008; Vidal et al., 2010) released by Météo-France are used (see retrospective simulation in Figure(see Fig. 1). Seyedhashemi et al. (2022b) already used this set-up and resulting outputs to estimate the magnitude of past trends in Q and Tw at the seasonal and annual scales. Figure ?? shows the period concerned by this retrospective simulation., and then averaged over each sub-basin. Finally, to have daily Q at the reach scale, simulated Q at the sub-basin outlets is redistributed along the river network inside each sub-basin according to each reach drainage area (through a routine in T-NET).

2.2 Calibration and validation of EROS

EROS had been calibrated over 1974-2018 to maximize the number of streamflow discharge near-natural observations, with 1971–1974 used for the warm-up. The calibration optimized all unknown parameters (soil capacity, recession times, and propa-
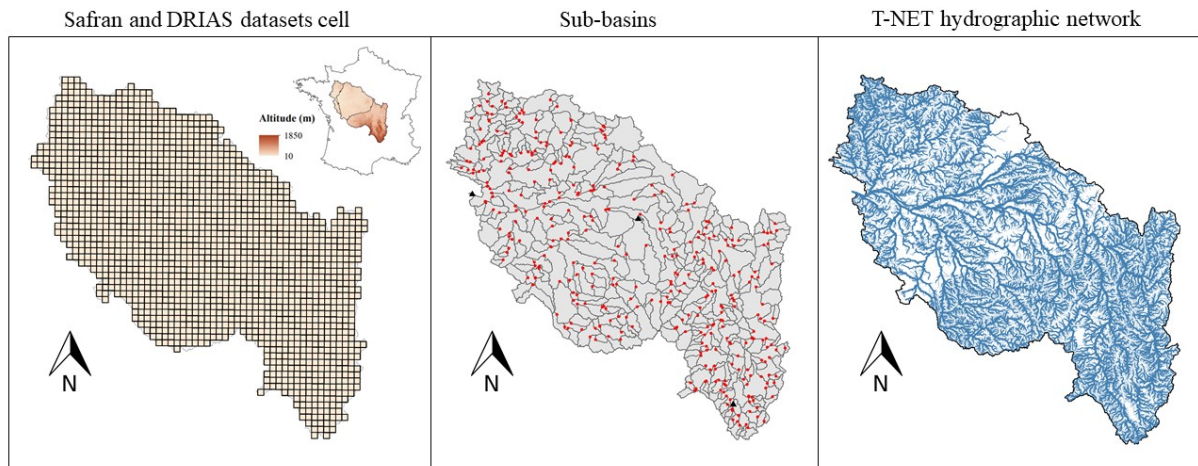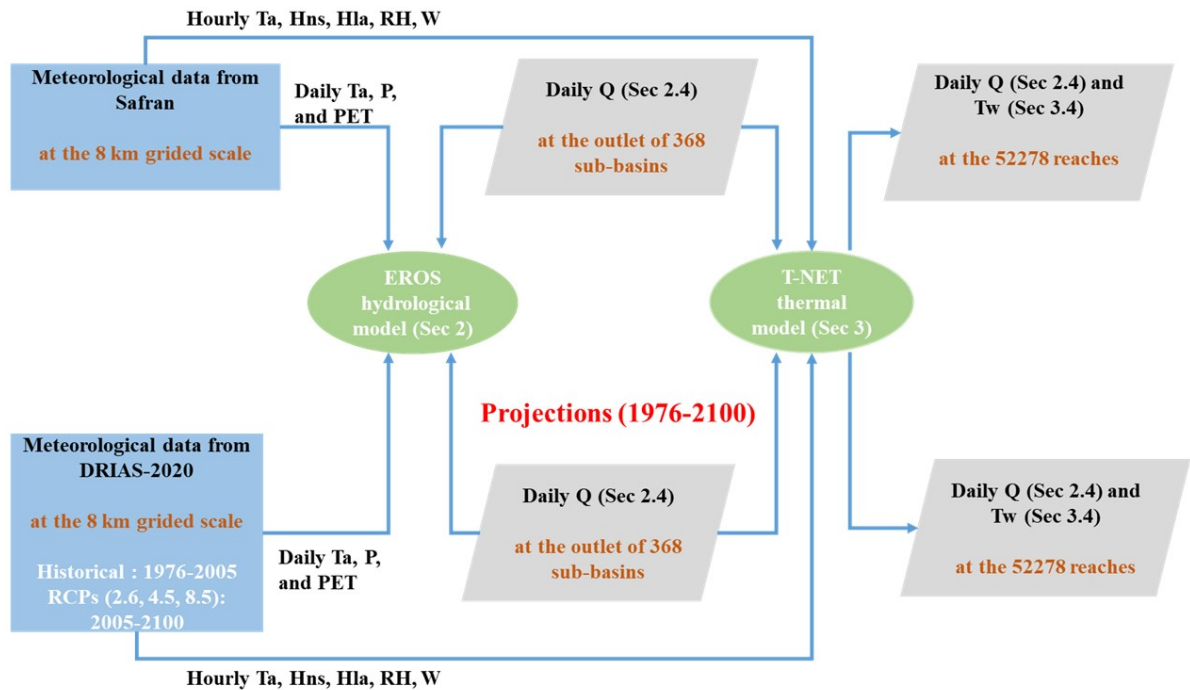
Figure 1. Synthetic diagram showing the methodology of retrospective simulations and projections of daily Q and Tw over the Loire River basin as well as the spatial resolution of input data in each step. The red circle points in the map of sub-basins show the outlets of 368 sub-basins while the three black triangle points show the position of sub-basin examples in the southern (L'Allier at Monistrol-d'Allier), the middle (L'Arnon at Méreau [Pont de Méreau]) and the northern part (La Loire at Montjean) of the basin used in the text.

gation times) through maximizing the Nash-Sutcliffe Efficiency (NSE) criterion on the square root of ~~streamflow~~ discharge and

90 minimizing the overall bias ~~(Seyedhashemi et al., 2022b, see)~~ (see Seyedhashemi et al., 2022b). Seyedhashemi et al. (2022b) validated and assessed the performance of the EROS through computing seasonal and annual relative biases, together with Nash–Sutcliffe efficiency on Q, $ln(Q)$, and $\sqrt{Q}$ over the 1963-2019 period. In a majority of calibration stations (75%), and stations on the French Reference Hydrometric Network (83%), NSE is > 0.7 for all Q, $ln(Q)$, and $\sqrt{Q}$. EROS performed well at the annual scale (median relative bias=0%) while it slightly underestimated winter (-6.27%) and spring Q (-3.47%), and

95 overestimated summer (+34.7%) and autumn Q (+20.9%) (see Fig. S6 of Seyedhashemi et al., 2022b). Such an overestimation in Q over summer and autumn was attributed to the fact that EROS does not consider the influence of water abstractions and impoundments. Moreover, significant spatial correlation (p<0.05) between seasonal Q trends in retrospective simulation against observations at hydrometric stations with long-term continuous daily data were also noted (see Fig. S10 of Seyedhashemi et al., 202 .

100 **2.3 Projections (~~1976–2100~~1976-2100)**

~~The DRIAS2020~~ For future projections of daily Q, EROS uses meteorological data provided by the DRIAS-2020 climate projection dataset ~~(Soubeyroux et al., 2020) has been recently~~ which has been released over France through the DRIAS portal (see http://www.drias-climat.fr/) (Soubeyroux et al., 2020). It comprises an ensemble of climate projections under 3 Representative Concentration Pathways used in the fifth IPCC Assessment Report (Core Writing Team et al., 2015) derived from the larger

105 EUROCORDEX dataset using Regional ~~Climaet~~ Climate Models (RCM) over Europe. This ensemble ~~id~~ is downscaled over France to the ~~8-km~~ 8 km Safran grid and bias-corrected with respect to the Safran reanalysis data with the ADAMONT method (Verfaillie et al., 2017). In this study a subset of 3 contrasted future ~~projections~~ climate models (GCM+RCM) are used to sample the dispersion of the full ensemble of 12 GCM+RCM projections from the ~~DRIA2020~~ DRIAS-2020 dataset. The 3 ~~selected projections~~ future climate models include a warm and wet couple of models (IPSL-CM5A/MRWRF381P), an intermediate one

110 (CNRM-CM5-LR/ALADIN63), and a hot and dry couple (HadGEM2/CCLM4-8-17).

All ~~these three GCM/RCMs~~ 3 selected future climate models (GCM+RCM) include RCP 4.5 and 8.5, which are intermediate and extreme scenarios corresponding to a plausible representation of the future behavior of human societies. The CNRM-CM5-LR/ALADIN63 model also includes RCP 2.6. Therefore, the projections are conducted under 7 projections in total~~(total= (2 GCM/RCMs × 2 RCPs) + (1 GCM/RCM × 3 RCP)= 7 projections)~~. For each GCM~~/RCMs, there are two periods of data~~+RCM,

115 two periods are considered: 1) the period with GCMs forced by historical concentrations in greenhouse gases between 1976 and 2005, and 2) the projection part using RCPs as forcings, which extends from 2005 to 2100 (see Table 1, and projections in ~~Figure~~Fig. 1 and ~~Figure ??~~Fig. S1). It should be noted that, although selected ~~GCM/RCMs have data from~~ projections start in the 1950s, ~~both hydrological and thermal models~~ hydrological model in the current study are ~~used~~ forced from the 1970s ~~,~~ onwards.

120 ~~The meteorological variables~~ Daily Ta, P and PET provided by these 7 projections are integrated into ~~both the EROSand T-NET models as explained in section ?? (see also Figure 1). Both the~~ EROS~~and T-NET models are~~. It then produces daily Q under each projection over the historical period (1976–2005) and the future (2005–2100) ("Projections" in Fig. 1). Note

Table 1. ~~The GCM/~~GCMs, RCMs, and RCPs used in ~~the~~ current study~~study~~. More information can be found in http://www.drias-climat.fr/.

GCM	RCM	~~HISTO~~ HIST	RCP 2.6	RCP 4.5	RCP 8.5	~~Data period~~ Period
IPSL-CM5-MIR	**WRF381P**	✓		✓	✓	1976-2005; 2006-2100
Dufresne et al. (2013)	Skamarock et al. (2008)					
Hourdin et al. (2013)						
CNRM-CM5	**ALADIN63 V2**	✓	✓	✓	✓	1976-2005; 2006-2100
Voldoire et al. (2013)	Colin et al. (2010)					
	Bador et al. (2017)					
HadGEM2-ES	**CCLM4-8-17**	✓		✓	✓	1976-2005; 2006-2099
Jones et al. (2011)	Keuler et al. (2016)					

that PET in DRIAS-2020 is computed by a Penman–Monteith equation using a proxy for radiation (calculated by maximum and minimum Ta), in order to use neither GCM+RCMs radiation nor Safran radiation for the bias correction (see http://

125 www.drias-climat.fr/accompagnement/sections/310 for PET calculation in projections). This PET equation is therefore slightly different from the one used for calibrating EROS. Note also that EROS is calibrated and run under present land cover/land use~~while calibrated parameters of EROS are kept as for the retrospective simulation (see Seyedhashemi et al. (2022b) for short description of calibration)~~. ~~The EROS model is first executed to produce daily Q under each projection over the historical period (~~

130 To assess future projections of Q in the present-day and their biases, we consider daily Q retrospective simulations (under Safran reanalysis) at the sub-basins outlets as the reference data and compared them with projections under DRIAS-2020 dataset over the 1976–2005 ~~) and the future (2005–2100)~~. ~~Indeed, for each projection, the EROS model is run from the 1976 to the 2100 while for RCPs of each GCM/RCM, the historical part (~~period over summer period. The 1976–2005 ~~) is the same (see projections in Figure 1, and Figure ??). Then, future daily Q and meteorological variables provided by GCM/RCMs are used~~

135 ~~in the T-NET thermal model to produce daily Tw under these future climate projectionsover the whole century (1976–2100)~~. ~~It should be noted that like projected Q, for RCPs of each GCM/RCM, projected Tw over the historical part (1976–2005)is the same (see projections in Figure 1, and see Figure ??).~~ period is the reference period used to correct the biases of climate projections with respect to Safran in the DRIAS-2020 dataset.

3 ~~Data assessment and overall description~~

140 ## 2.1 Data description over the summer period (June-August)

~~Although the time series of both Q and Tw are available for the whole year, here, we mainly focus on June to August months (hereafter referred to as summer) , the time of the year which is vital for the survival (Steel et al., 2017), growth and migration of aquatic communities (Arevalo et al., 2020).~~

Retrospective simulation (1963-2019)

145 **2.2** ~~**Retrospective simulation (1963–2019)**~~

~~**Streamflow**~~

~~The performance of the EROS model in simulating daily Q over the Loire River basin was assessed in a previous paper (Seyedhashemi et al., 2022b).In a majority of calibration stations (75%), and stations on the French Reference Hydrometric Network (83%), the Nash-Sutcliffe efficiency of simulated daily Q is > 0.7 for Q, $ln(Q)$, and $\sqrt{Q}$. At the seasonal scale and at~~
150 ~~natural calibration stations~~ Trends in Q over the ~~Loire River basin, the EROS model performed well at the annual scale while it slightly underestimated winter and spring Q, and overestimated summer and autumn Q (see Figure S6 Seyedhashemi et al., 2022b) . Such an overestimation in Q over summer and autumn is attributed to the fact that EROS does not consider the influence of water abstractions and impoundments (see section ??). Significant correlations between seasonal Q trends in retrospective simulation against observations at hydrometric stations with long-term continuous daily data were noted (see Figure S10 Seyedhashemi et a~~
155 ~~.~~

~~Lastly, decreasing Qtrends were detected in the southern part of the basin (in the Massif central)over the 1963–2019 period (up to~~ 1963–2019 period are highly variable in magnitude and direction across the basin, with decreasing Q in the southern part of the basin (in the Massif Central up to ~~-16 %/decade)~~ ~~while mainly increasing Q trends was found in the remaining parts of the basin (see Figure 3 Seyedhashemi et al., 2022b). Figure 2, left panel, shows such~~ and increasing Q in the remaining parts of
160 the basin (see Fig. 3 of Seyedhashemi et al., 2022b). Similarly, retrospective simulation in Fig. 2 shows a decrease in summer Q for a ~~decrease in summer Q for a~~ sub-basin in the ~~southern part while summer Q is relatively stationary at the~~ southern part while the same variable is relatively stationary at the other two sub-basins ~~in the middle and northern part. It should be noted EROS performed well in reconstructing daily Q at the outlet of these 3 sub-basins (see Figure S8 Seyedhashemi et al., 2022b) .~~ in the middle and northern part. Seyedhashemi et al. (2022b) also found that the seasonal and annual anomalies of Q show a
165 relatively stationary evolution with -100% to 150% values in summer across the basin (their Fig. S17).

Projections (1976-2100)

~~**Stream temperature**~~

~~A~~ Projections underestimate summer Q (up to -45% depending on GCM+RCM) mainly in the middle and north part of the basin, and overestimate summer Q in the southern part of the basin (Figure 3). An overestimation can be found over the
170 whole basin for HadGEM2/CCLM4-8-17. Such differences between simulations and projections can be due to differences in
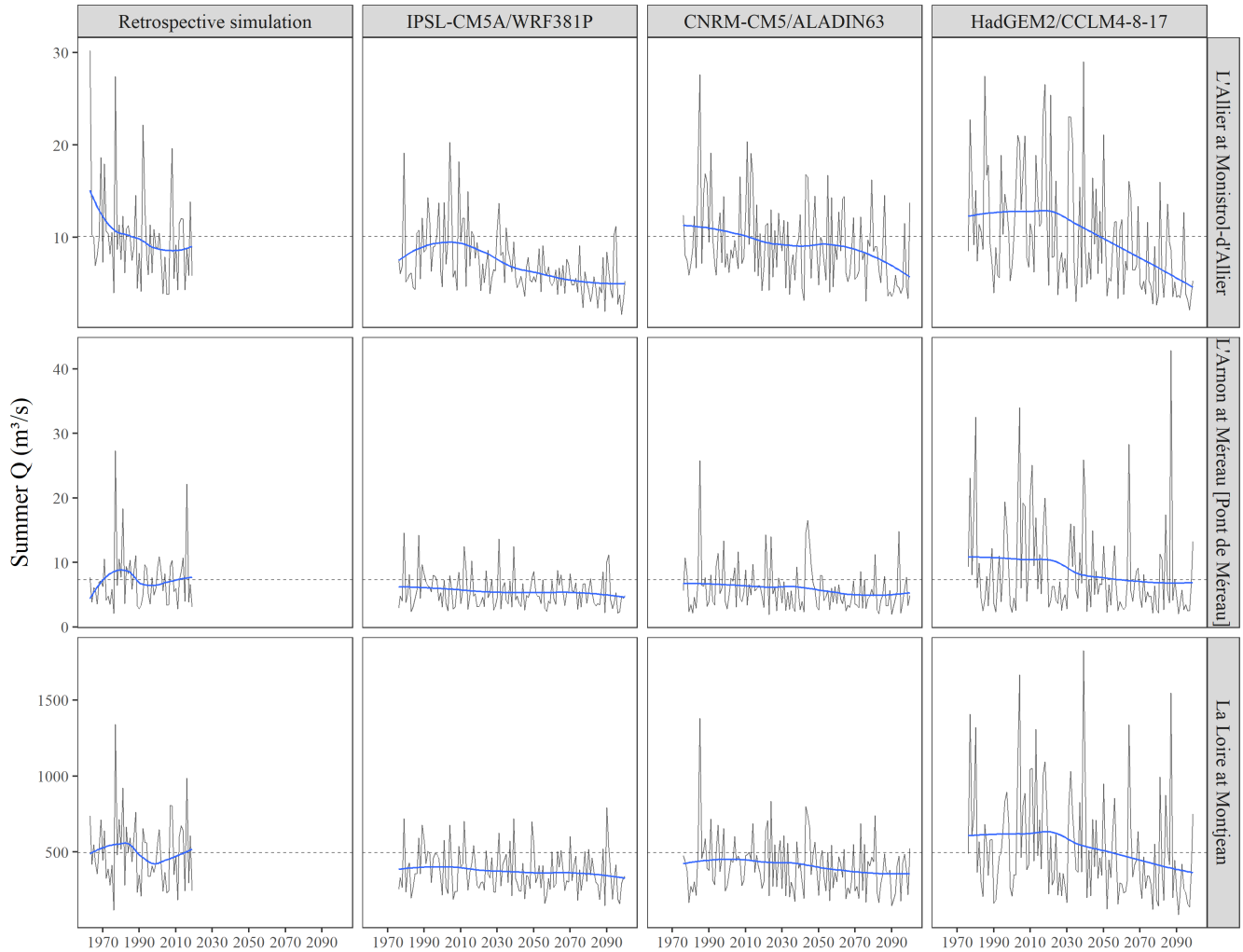
Figure 2. Summer Q in retrospective simulation and projections under RCP 8.5 for 3 sub-basins in the southern (L'Allier at Monistrol-d'Allier), middle (L'Arnon at Méreau [Pont de Méreau]) and northern part (La Loire at Montjean) of the Loire basin as shown in Fig. 1. The dashed line represents the average of summer Q in the retrospective simulation over the 1963–2019 period. Blue lines roughly show the temporal evolution using local regression models. It should be noted that EROS performs well in reconstructing daily Q at the outlet of these 3 sub-basins (see Fig. S8 of Seyedhashemi et al., 2022b).

PET calculation between the retrospective simulation and projections, as well as the specifics of the bias-correction method (Soubeyroux et al., 2020).
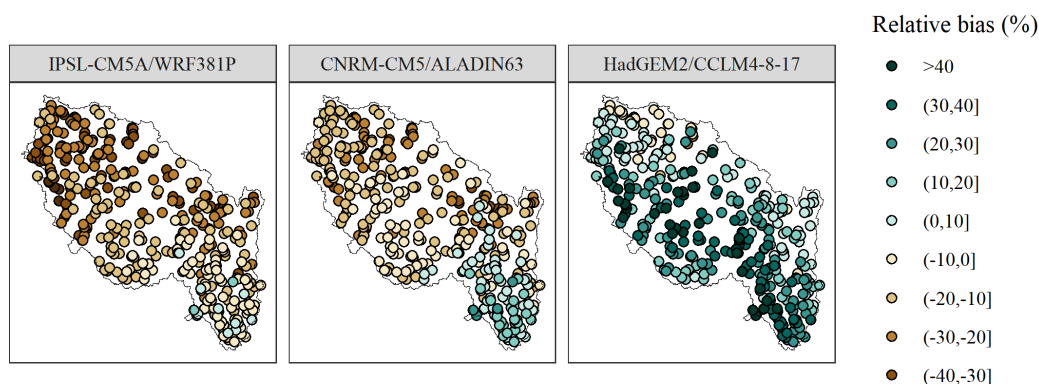

Figure 3. Map of relative biases between summer Q in projections and in the retrospective simulation at the outlet of 368 sub-basins over the 1976–2005 period.

In the southern (L'Allier at Monistrol-d'Allier) and northern parts (La Loire at Montjean) of the basin, summer Q is decreasing in 21st century projections regardless of the GCM+RCM, with the largest decrease for HadGEM2/CCLM4-8-17 (Fig. 2). However, such a decrease is limited in the middle part of the basin (L'Arnon at Méreau [Pont de Méreau]). Figure 4 shows that for IPSL-CM5A/MRWRF381P, there is a north-to-south and increase-to-decrease gradient in the middle of the century (2040–2069) with respect to the present time (1990–2019) under RCP 8.5. There is also a decrease in the downstream part of the basin for HadGEM2/CCLM4-8-17 and to a lesser extent for CNRM-CM5-LR/ALADIN63. However, for the latter, an increase in summer Q is observed in some parts in the south while for HadGEM2/CCLM4-8-17, a decrease in summer Q is projected for the whole basin with the greatest decrease in the southern part (Fig. 4).

Under RCP 8.5, the annual regime of projected Q will be also different from one GCM+RCM to another, and from one sub-basin to another (see Fig. S2). For instance, at a sub-basin in the southern part of the basin (L'Allier at Monistrol-d'Allier), the highest Q is projected by HadGEM2/CCLM4-8-17 over spring while this happens over winter for IPSL-CM5A/MRWRF381P for a northern sub-basin (La Loire at Montjean). Nevertheless, for both sub-basins, the annual regime of Q for HadGEM2/CCLM4-8-17 under RCP 8.5 shows that the low-flow period lasts longer (even until fall) compared to the two other model combinations.

3 T-NET thermal model and daily stream temperature data

3.1 Principles and input of T-NET

To estimate daily Tw for 52 278 reaches (median length=1.3 km) over the Loire River basin, T-NET calculates the equilibrium temperature and solves the local heat budget while assuming steady-state conditions and accounting for confluence thermal signal mixing with respect to discharges. The equilibrium temperature is defined as the temperature at which the total heat
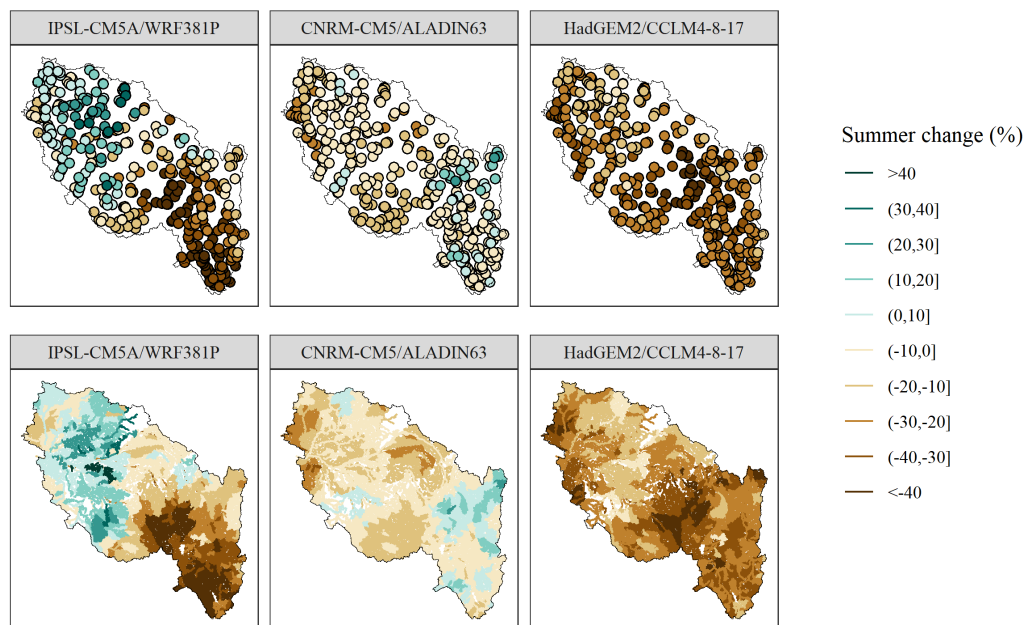
Figure 4. Changes in summer Q with respect to the 1990–2019 period in the middle of the century (2040–2069) for all GCM+RCMs under RCP 8.5 at the outlet of 368 sub-basins and and at the reach scale (for 52 278 reaches).

fluxes at the water body is 0 (see equations 1 and 2 of Beaufort et al., 2016a). The heat fluxes include net solar radiation, atmospheric longwave radiation, longwave radiation emitted from the surface water, evaporative heat flux, convective heat flux, and groundwater flux. T-NET also simulates the Tw longitudinal variation and upstream-downstream thermal propagation through water travel time (TT).

To compute the six heat fluxes and the water travel time for each reach, Q at the reach scale is used in a hydraulic geometry model assuming a rectangular river section to simulate water depth (H), width (W) and velocity (V). Then, to estimate hourly Tw at each reach, T-NET uses these estimated Q, H, W and TT (the ratio of reach length to water velocity) as well as Ta, shortwave net solar radiation (Hns), longwave radiation (Hla), specific humidity (RH), and wind velocity (W), and riparian shading (as a function of vegetation density, solar elevation angle, tree height, river width, and phonology) at hourly time step (see Seyedhashemi et al., 2022b, for more detailed information). Meteorological variables such as Ta, Hns, RH, and W are provided by the 8 km Safran grid. All reaches within a grid cell are attributed meteorological data values for that cell. For reaches flowing through more than one grid cell, meteorological variables are weighted by the relative length of the reach within each grid cell (Seyedhashemi et al., 2022b). Finally, hourly outputs of T-NET are averaged on a daily scale to have daily Tw.

3.2 Validation of T-NET

Unlike EROS, T-NET does not have any free parameters, and hence it is not calibrated. A validation was already done by Seyedhashemi et al. (2022b) over the 2010–2014 period at 67 near-natural observational stations with continuous daily data, which were also weakly influenced by impoundments (spotted through the "thermal signatures" approach in Seyedhashemi et al., 2020). A small underestimation in seasonal Tw (median range: -0.29 °C to +0.15 °C) on large rivers was found ~~in a previous paper~~

210 ~~(see Figure S9 Seyedhashemi et al., 2022b)~~(see Fig. S9 of Seyedhashemi et al., 2022b). Indeed, 3 ~~%~~ to 83 ~~%~~ % of stations (resp. 50 ~~%~~ to 100 %) on small and medium (resp. large) rivers had a RMSE < 1 °C across seasons (see their ~~Figure~~Fig. S9, bottom panel). A significant spatial correlation between seasonal and annual Tw trends in retrospective simulations against observations was also found at Tw stations with long-term continuous daily data (see Fig. S11 of Seyedhashemi et al., 2022b). At the seasonal and annual scales, a strong temporal coherence and agreement between observations and reconstruction ~~was~~

215 were also found for the four stations along the main stem of the Loire River with the long-term data ~~(see Figure 2 Seyedhashemi et al., 2022b~~ ~~. A significant correlation between seasonal and annual Tw trends in retrospective simulations against observations were also found at Tw stations with long-term continuous daily data (see Figure S11 of Seyedhashemi et al., 2022b).~~ (see Figure 2 Seyedhashemi et al

~~A Tw increase was also detected for almost all reaches in all seasons (mean=+0.38 °C/decade) over the 1963–2019. Indeed,~~

220 ~~the median summer Tw over the basin has increased by +0.44 °C/decade (i.e. +2.5 °C over the whole 1963–2019 period) (according to Seyedhashemi et al., 2022b). Such a consistent increase in summer Tw in retrospective simulations can be also seen in Figure 7, top panel. Nevertheless, the mean summer Tw in the retrospective simulation remains rather low (< 18 °C) across the basin and only 14 % of reaches in retrospective simulation have a summer Tw > 18 °C (Figure 8).~~

~~Time series of summer Tw in retrospective simulation and projections. The solid line and shaded area represent the median~~

225 ~~and the 10th-90th percentile band over all 52 278 reaches, respectively. The dashed lines show the average of the median summer Tw values (solid line) in the retrospective simulation over the 1963–2019 period.~~

~~Spatial variability of summer Tw in the retrospective simulation over the 1963–2019 period and in projections for all GCM/RCMs under RCP 8.5 in the middle of century (2040–2069). Figure S2 presents the same spatial variability at the end of the century (2070–2099).~~

230 ~~Figure 5 , left panel shows a pretty~~ Figure 5 also shows a good performance of ~~the~~ T-NET ~~model~~ in reconstructing daily Tw at the Avoine on the Loire River (uninfluenced by human impacts) in 2003, the hottest year in the recent period (Moatar and Gailhard, 2006; Bustillo et al., 2014; Seyedhashemi et al., 2022b). Although there is a ~~good coherence~~ small bias (0.7 °C) between simulations and observations over the year~~(Bias=0.7 °C)~~, an overestimation in simulation (2.5 °C) is observed at the day with maximum daily Tw. ~~Beaufort et al. (2016a) showed that the Root Mean Square Error (RMSE) of the T-NET model~~

235 ~~in simulating daily Tw was on average 1.60 °C at 128 natural stations with missing years over the 2008–2012 period over the Loire River basin. Over this basin, the RMSE of the T-NET model in simulating daily Tw at 275 natural stations with missing years over the 2008–2018 period (spotted through "thermal signatures" approach in Seyedhashemi et al., 2020) is 1.80 °C.~~

~~In 2003, the majority of reaches (76 %) had a maximum daily Tw > 22 °C, and 49% of reaches showed maximum daily Tw > 24 °C (Figure 5, right panel).~~ The maximum observed daily Tw ~~in the downstream part of the Loire river at Avoine~~ at

240 Avoine in 2003 is 31 °C ~~in 2003 (see Figure 5, left panel~~(see Fig. 5). Such a value is expected to be seen at rivers with low
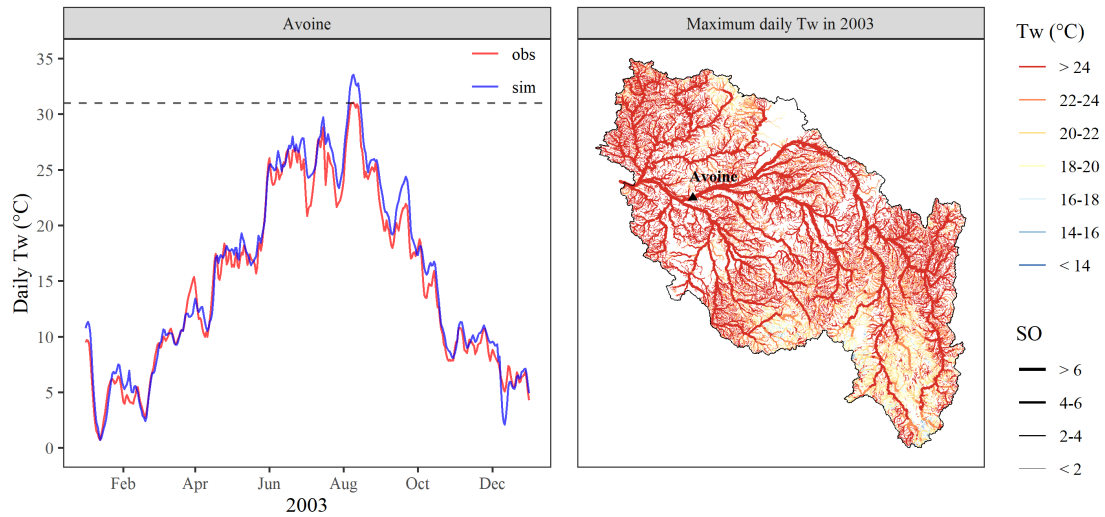
Figure 5. ~~(left)~~ Observed and simulated daily Tw at Avoine on the downstream part of the Loire River in 2003. The dashed line shows the maximum daily Tw over observed data at Avoine. ~~(right) Simulated~~ The map of simulated maximum daily Tw in ~~2003.~~ 2003 for the whole 52 278 reaches is also presented with the line size showing the Strahler order of the reach. The black triangle shows the position of Avoine on the Loire River. ~~The line size shows the Strahler order of REACHED.~~

velocity and shallow water ~~such as Avoine is located on a large river (SO=8)~~, which are mainly large rivers (OS $\geq$ 7) like the river of Avoine station. However, all of 470 reaches with at least one day with Tw $> 31\,°C$ in 2003 are not located on large rivers (see ~~Figure~~Fig. 6). 57 % of such reaches have a Strahler order between 5 and 6, and 12 % have a Strahler order less than 5 ~~(see Figure 6)~~, indicating an overestimation in maximum daily Tw ~~.~~ (see Fig. 6).

3.3 Projections (~~1976–2100~~1976-2100)

~~Streamflow~~

~~In the southern (L'Allier at Monistrol-d'Allier) and northern part (La Loire at Montjean) of the basin, summer Q is decreasing in projections regardless of the GCM~~For future projections of daily Tw, T-NET uses the meteorological variables (Ta, Hns, RH, and W) at the hourly step under 7 projections described in Sect. 2.3 (see also Table 1). Like EROS, T-NET is run under present land cover/~~RCM, with the largest decrease under the HadGEM2/CCLM4-8-17 model combination. However, such a decrease is limited in middle part of the basin (L'Arnon at Méreau Pont de Méreau) (Figure 2). Under the IPSL-CM5A/MRWRF381P model, there is a north-to-south and increase-to-decrease gradient in the middle of the century (2040–2069) with respect to the present time (1990–2019) (Figure 4). There is also a decrease in the downstream part of the basin under the HadGEM2/CCLM4-8-17 model and to a lesser extent under the CNRM-CM5-LR/ALADIN63 model.However, under the later,~~ land use. To assess future projections of Tw in present-day, we follow the same approach as for Q (see Sect. 2.3). We consider daily Tw retrospective

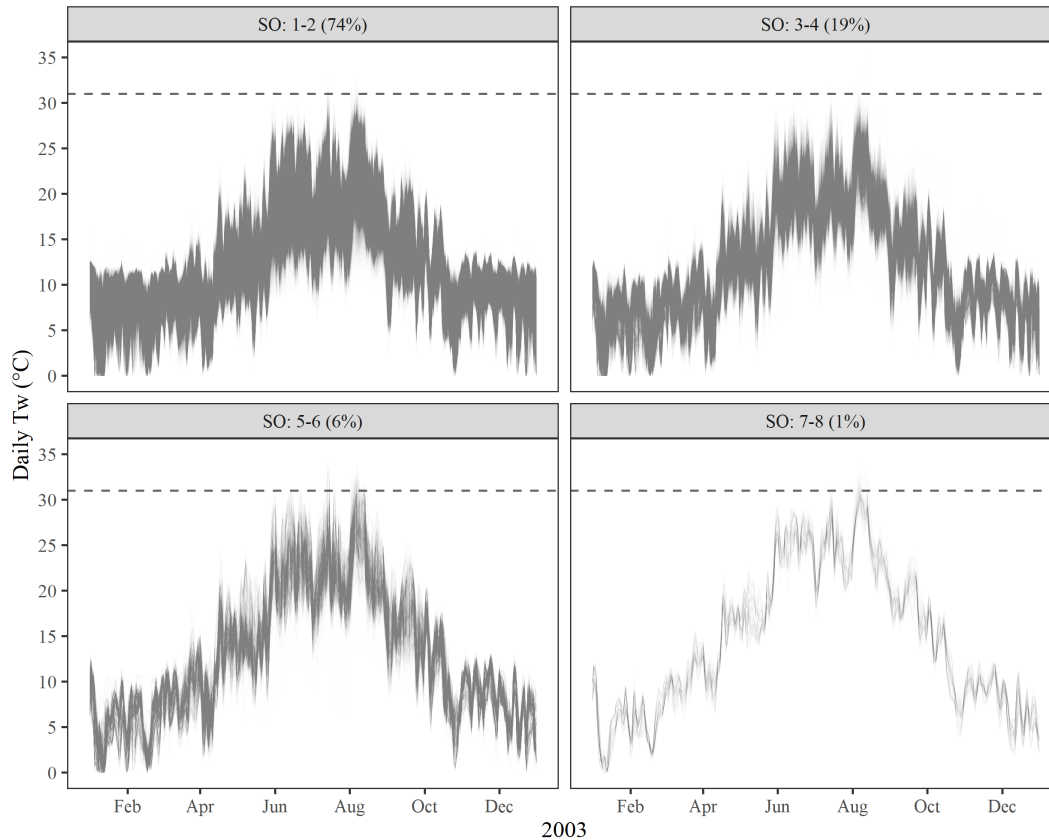**Figure 6.** Simulated ~~daily~~ Tw for reaches with different Strahler orders (SO) in 2003. Each curve corresponds to the daily Tw time series of one of the 52 278 reaches in the basin. The dashed line shows the maximum observed daily Tw at Avoine on the Loire River (see Figure 5)~~Figure 5, left panel~~ which is ~~indeed an example of daily Tw time series shown in this figure, bottom right panel for OS~~a large river with SO ≥ 7. Panel titles give the percentage of reaches within each SO class.

simulation (under Safran reanalysis) for 52 278 reaches as the reference data and compared them with projections from the DRIAS-2020 dataset over the 1976–2005 period over summer period.

3.4 Data description over the summer period (June-August)

Retrospective simulation (1963-2019)

260 An increase in Tw was detected for almost all reaches in all seasons (mean=+0.38 °C/decade) over 1963–2019 by Seyedhashemi et al. (202? with a median increase in summer Tw over the basin by +0.44 °C/decade (i.e. +2.5 °C over the whole 1963–2019 period). Such a consistent increase in summer ~~Q is observed in some parts in the south while under the HadGEM2/CCLM4-8-17 model, a decrease in summer Q is projected for the whole basin with the greatest decrease in the southern part of the basin (Figure 4~~Tw

13

in retrospective simulations can be also seen in Fig. 7. Nevertheless, only 14 % of reaches in retrospective simulation have an

265   average summer $Tw > 18\,°C$ (Fig. 8). In 2003, the hottest year in the recent periods, the majority of reaches (76 %) have a maximum daily $Tw > 22\,°C$, and 49% of reaches show a maximum daily $Tw > 24\,°C$ (Fig. 5).
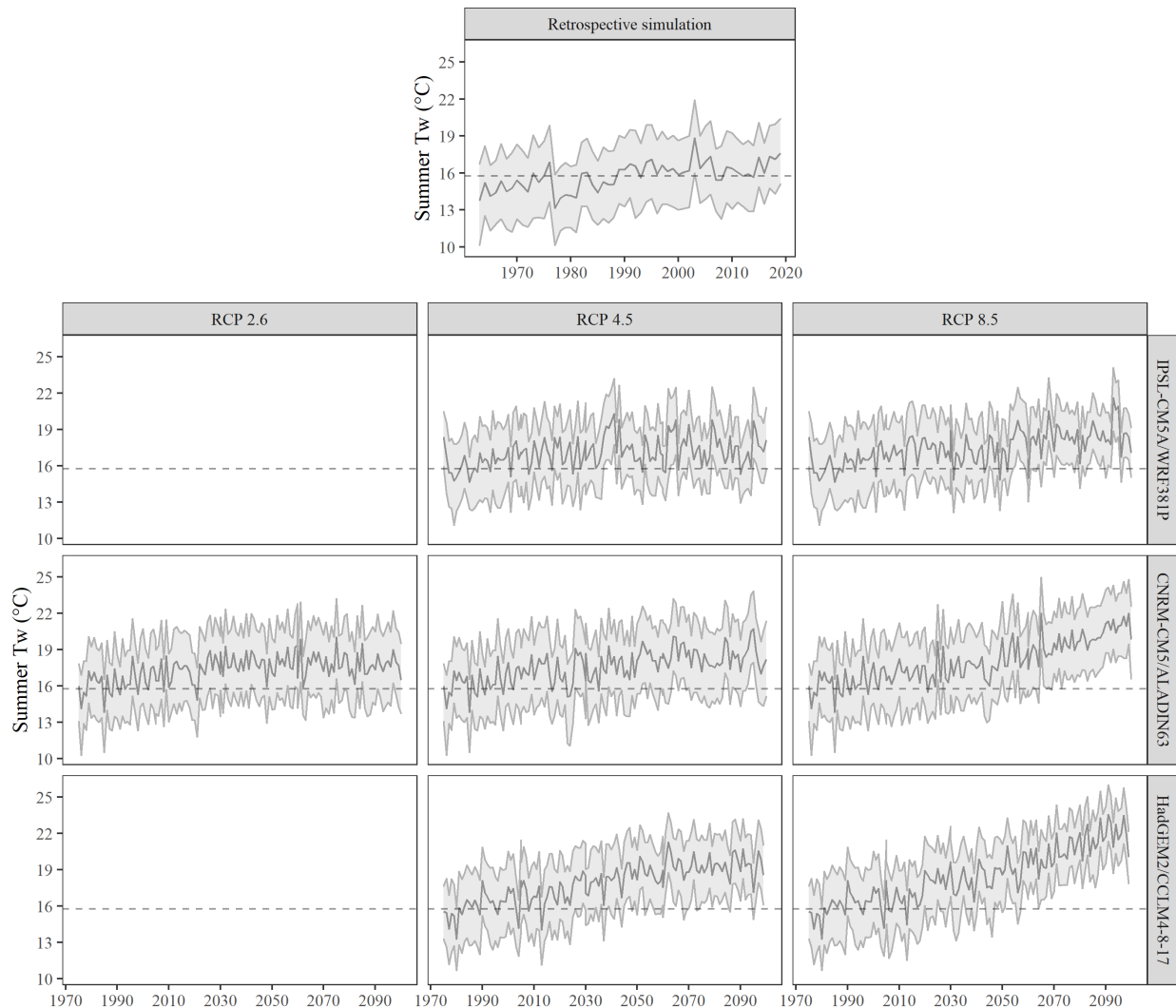

Figure 7. ~~Changes in~~ Time series of summer ~~Q with respect to the 1990–2019 period~~ Tw in retrospective simulation and projections. The solid line and shaded area represent the ~~middle of~~ median and the ~~century (2040–2069) for~~ 10th-90th percentile band over all ~~GCM/RCMs~~ ~~under RCP 8.5 (top) at~~ 52 278 reaches, respectively. The dashed lines show the ~~outlet~~ average of ~~368 sub-basins and~~ the median summer Tw values (~~bottom~~solid line) ~~at~~ in the ~~reach scale~~retrospective simulation over the 1963–2019 period.

14

~~Under RCP 8.5, the annual regime of projected Q will be also different from one GCM/RCM to another, and from one sub-basin to another (see Figure S1). For instance, at a sub-basin in the southern part of the basin (L'Allier at Monistrol-d'Allier), the highest Q is projected under the HadGEM2/CCLM4-8-17 model over spring while this happens over winter period under the IPSL-CM5A/MRWRF381P model for a sub-basin in the northern~~

Projections (1976-2100)

There is a slight overestimation of Tw across GCMs+RCMs over 1976-2005 (median bias=0.2 °C- 0.4 °C, and see Fig. 9). The Interquartile Range (IQR) remains small (0.2 °C) and similar across GCMs+RCMs. Across GCMs+RCMs, the largest biases are found in the northeast part of the basin ~~(La Loire at Montjean). Nevertheless, for both sub-basins, the annual regime of Q under the~~ and in some middle reaches. The underestimation in Tw occurs partially for reaches in the higher altitudes mostly for HadGEM2/CCLM4-8-17 ~~model and RCP 8.5 shows that the lowflow period lasts longer (even until fall)compared to other two models~~(Fig. 9).

~~Stream temperature~~

Time series of all reaches under all ~~GCM/~~GCMs+RCMs show a consistent increase in summer Tw from the past to future under RCP 8.5 (~~see Figure~~Fig. 7). Under this RCP, summer anomalies at the end of the century with respect to ~~1963-2019 ranges~~ 1963–2019 range, are on average, between 5.8 °C and 7.8 °C depending on ~~GCM/RCMs, in average over the basin at the end of the century~~GCMs+RCMs. Conversely, summer Tw under RCP 2.6 and 4.5 ~~are~~ is more stable after 2050 (~~Figure~~Fig. 7). Nevertheless, under these two RCPs, anomalies from 2050 onwards are yet quite large (4.2 °C to 4.7 °C depending on ~~GCM/~~GCMs+RCMs and RCP). These overall conclusions are exemplified in ~~Figure~~Fig. S3.

Figure 8 shows a considerable increase in mean summer Tw in the middle of the century (2040–2069) compared to the retrospective simulation over the 1963–2019 period. Only 14 % of reaches ~~had~~ has a mean summer Tw > 18 °C over the 1963-2019 period while in the middle of century, their number is expected to reach 42-73 % ~~of reaches exhibit a mean summer Tw > 18 °C~~ depending on the GCM/+RCM and RCP. Indeed, the frequency of reaches with Tw > 18 °C is increasing (57-96 % of reaches) towards the end of the century, with the exception of ~~the~~ IPSL-CM5A/MRWRF381P ~~model~~ under RCP 4.5 and ~~the~~ CNRM-CM5-LR/ALADIN63 ~~model~~ under RCP 2.6 (see ~~Figure S2~~Fig. S4). For the three selected sub-basins, an increase in the frequency of days Tw > 25 °C is also found towards the end of the century regardless of GCM/+RCM under RCP 8.5 with the largest values at the end of the century (> 50 days; see ~~Figure S4~~Fig. S5).

4 ~~Caveats~~

~~The Nash-Sutcliffe efficiency of reconstructed daily Q by the hydrological model was pretty good and > 0.7 for Q, $ln(Q)$, and $\sqrt{Q}$ (Seyedhashemi et al., 2022b). Nevertheless, there was an overestimation in summer and fall Q (Seyedhashemi et al., 2022b) as the EROS hydrological model does not consider the influence of water-abstractions and impoundments. Therefore, the users should be careful with this on highly regulated rivers. On the other hand, The RMSE of the thermal model in simulating~~
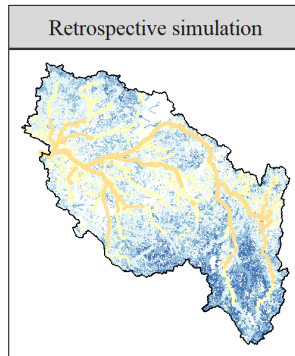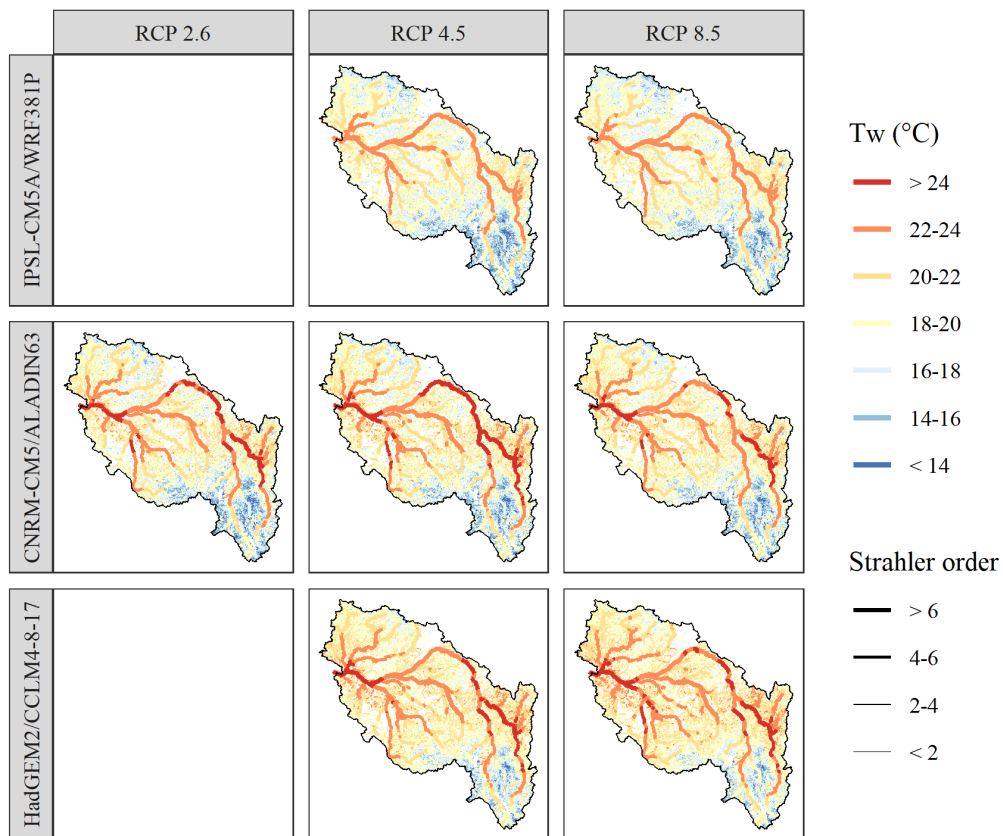
Figure 8. Spatial variability of average summer Tw in the retrospective simulation over the 1963–2019 period and in projections for all GCMs+RCMs under RCP 8.5 in the middle of the century (2040–2069). Figure S3 presents corresponding results at the end of the century (2070–2099).
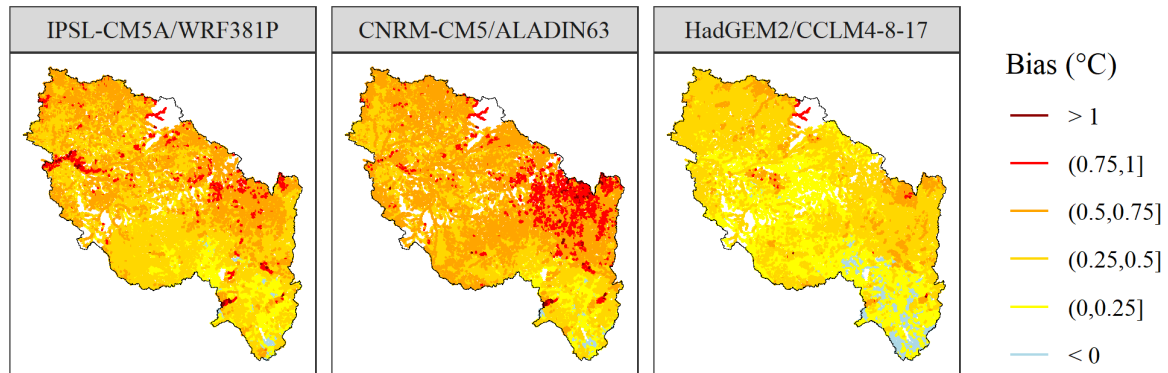
Figure 9. Map of summer TW biases between projections and the retrospective simulation over the 1976–2005 period.

4 Conclusion

This data paper presented and described daily Q and Tw reconstructions over the 1963–2019 period as well as projections over the 1976–2100 period for 52 278 reaches over the Loire River basin (10^5 km^2) using a physical process-based T-NET thermal model coupled with the EROS hydrological model.

Daily Q and Tw are projected under three contrasted downscaled and bias-corrected climate projections (~~GCM/RCM~~GCMs+RCMs) including warm and wet (IPSL-CM5A/~~MR~~WRF381P), intermediate (CNRM-CM5-LR/ALADIN63), and hot and dry (HadGEM2/CCLM4-8-17) models from the DRIAS-2020 dataset (Soubeyroux et al., 2020), under three Representative Concentration Pathways (RCPs) from the fifth report of IPCC (Core Writing Team et al., 2015). All of these three GCM/+RCMs were run under ~~RCP4.5 and RCP8.5, and the~~ RCP 4.5 and RCP 8.5, and CNRM-CM5-LR/ALADIN63 ~~model~~ was also run under RCP 2.6.

The potential applications of the proposed dataset over the past and future are manifold. This can be employed to understand spatio-temporal variability in Q and Tw, to assess the synchronicity of extermes ~~(e.g. studies of Arismendi et al., 2013; Arevalo et al., 2020)~~ (following e.g. Arismendi et al., 2013; Arevalo et al., 2020), to better explain and predict the possible spatial distribution of aquatic communities ~~(e.g. study of Picard et al., 2022, who used the current dataset)~~(following e.g. Picard et al., 2022, who used this speci , and to assess the various stresses on freshwater habitat due to climate change (e.g. Lee et al., 2020).

17

5 Data availability

~~The daily~~ Daily Q and Tw ~~in~~ for the retrospective simulation over the 1963–2019 period and ~~under~~ for the 7 projections over the 1976–2100 period are available for T-NET ~~hyrographic~~ hydrographic network (52 278 reaches) under the Attribution-NonCommercial 4.0 International (~~CC BY-NC~~ CC-BY-NC 4.0) in NetCDF file format through: ~~https://doi.org/10.57745/LBPGFS~~ https://doi.org/10.57745/LBPGFS (Seyedhashemi et al., 2022a). Ta and other ~~desired~~ meteorological variables corresponding to each reach can be extracted from the closest grid cell to the reach of the Safran reanalysis ~~database (~~ and the DRIAS-2020 projection dataset. Safran is available upon request from Météo-France ~~) for the retrospective simulation and of the~~ for research purposes. The DRIAS-2020 dataset ~~for projections (see DRIAS: http://www.drias-climat.fr/, portail partenarial Météo-France, IPSL, Cerfa~~ is freely available from the French national Climate Services Portal *DRIAS - Les futurs du Climat* http://www.drias-climat.fr/.

Author contributions. HS developed the dataset and prepared the manuscript. DT ran the EROS model and provided discharge data for both past and future. All co-authors contributed to the manuscript.

References

Allen, R. G., Pereira, L. S., Raes, D., and Smith, M.: Crop Evapotranspiration – Guidelines for computing crop water requirements, FAO Irrigation and Drainage Paper 56, FAO, http://www.kimberly.uidaho.edu/water/fao56/, 1998.

Arevalo, E., Lassalle, G., Tétard, S., Maire, A., Sauquet, E., Lambert, P., Paumier, A., Villeneuve, B., and Drouineau, H.: An innovative bivariate approach to detect joint temporal trends in environmental conditions: Application to large French rivers and diadromous fish, Science of the Total Environment, 748, 141 260, https://doi.org/10.1016/j.scitotenv.2020.141260, 2020.

Arismendi, I., Safeeq, M., Johnson, S. L., Dunham, J. B., and Haggerty, R.: Increasing synchrony of high temperature and low flow in western North American streams: double trouble for coldwater biota?, Hydrobiologia, 712, 61–70, https://doi.org/10.1007/s10750-012-1327-2, 2013.

Arora, R., Tockner, K., and Venohr, M.: Changing river temperatures in northern Germany: trends and drivers of change, Hydrological Processes, 30, 3084–3096, https://doi.org/10.1002/hyp.10849, 2016.

Bador, M., Terray, L., Boe, J., Somot, S., Alias, A., Gibelin, A.-L., and Dubuisson, B.: Future summer mega-heatwave and record-breaking temperatures in a warmer France climate, Environmental Research Letters, 12, 074 025, https://doi.org/https://doi.org/10.1088/1748-9326/aa751c, 2017.

Beaufort, A., Curie, F., Moatar, F., Ducharne, A., Melin, E., and Thiéry, D.: T-NET, a dynamic model for simulating daily stream temperature at the regional scale based on a network topology, Hydrological Processes, 30, 2196–2210, https://doi.org/10.1002/hyp.10787, 2016a.

Beaufort, A., Moatar, F., Curie, F., Ducharne, A., Bustillo, V., and Thiéry, D.: River temperature modelling by Strahler order at the regional scale in the Loire River basin, France, River Research and Applications, 32, 597–609, https://doi.org/https://doi.org/10.1002/rra.2888, 2016b.

Bustillo, V., Moatar, F., Ducharne, A., Thiéry, D., and Poirel, A.: A multimodel comparison for assessing water temperatures under changing climate conditions via the equilibrium temperature concept: case study of the Middle Loire River, France, Hydrological Processes, 28, 1507–1524, https://doi.org/https://doi.org/10.1002/hyp.9683, 2014.

Carlson, A. K., Taylor, W. W., Hartikainen, K. M., Infante, D. M., Beard, T. D., and Lynch, A. J.: Comparing stream-specific to generalized temperature models to guide salmonid management in a changing climate, Reviews in Fish Biology and Fisheries, 27, 443–462, https://doi.org/https://doi.org/10.1007/s11160-017-9467-0, 2017.

Colin, J., Déqué, M., Radu, R., and Somot, S.: Sensitivity study of heavy precipitation in Limited Area Model climate simulations: influence of the size of the domain and the use of the spectral nudging technique, Tellus A: Dynamic Meteorology and Oceanography, 62, 591–604, https://doi.org/https://doi.org/10.1111/j.1600-0870.2010.00467.x, 2010.

Core Writing Team, Pachauri, R. K., and Meyer, L. A., eds.: Climate change 2014: synthesis report. Contribution of Working Groups I, II and III to the fifth assessment report of the Intergovernmental Panel on Climate Change, IPCC, https://www.ipcc.ch/site/assets/uploads/2018/02/SYR_AR5_FINAL_full.pdf, 2015.

Cox, T. J. and Rutherford, J. C.: Predicting the effects of time-varying temperatures on stream invertebrate mortality, New Zealand Journal of Marine and Freshwater Research, 34, 209–215, https://doi.org/10.1080/00288330.2000.9516927, 2000.

Du, X., Shrestha, N. K., and Wang, J.: Assessing climate change impacts on stream temperature in the Athabasca River Basin using SWAT equilibrium temperature model and its potential impacts on stream ecosystem, Science of the Total Environment, 650, 1872–1881, https://doi.org/10.1016/j.scitotenv.2018.09.344, 2019.

Dufresne, J.-L., Foujols, M.-A., Denvil, S., Caubel, A., Marti, O., Aumont, O., Balkanski, Y., Bekki, S., Bellenger, H., Benshila, R., et al.: Climate change projections using the IPSL-CM5 Earth System Model: from CMIP3 to CMIP5, Climate dynamics, 40, 2123–2165, https://doi.org/https://doi.org/10.1007/s00382-012-1636-1, 2013.

Dugdale, S. J., Hannah, D. M., and Malcolm, I. A.: River temperature modelling: A review of process-based approaches and future directions, Earth-Science Reviews, 175, 97–113, https://doi.org/10.1016/j.earscirev.2017.10.009, 2017.

Elliott, J. and Elliott, J.: Temperature requirements of Atlantic salmon Salmo salar, brown trout Salmo trutta and Arctic charr Salvelinus alpinus: predicting the effects of climate change, Journal of fish biology, 77, 1793–1817, https://doi.org/https://doi.org/10.1111/j.1095-8649.2010.02762.x, 2010.

Hannah, D. M. and Garner, G.: River water temperature in the United Kingdom: changes over the 20th century and possible changes over the 21st century, Progress in Physical Geography, 39, 68–92, https://doi.org/10.1177/2F0309133314550669, 2015.

Hourdin, F., Foujols, M.-A., Codron, F., Guemas, V., Dufresne, J.-L., Bony, S., Denvil, S., Guez, L., Lott, F., Ghattas, J., et al.: Impact of the LMDZ atmospheric grid configuration on the climate and sensitivity of the IPSL-CM5A coupled model, Climate Dynamics, 40, 2167–2192, https://doi.org/https://doi.org/10.1007/s00382-012-1411-3, 2013.

Jones, C., Hughes, J., Bellouin, N., Hardiman, S., Jones, G., Knight, J., Liddicoat, S., O'connor, F., Andres, R. J., Bell, C., et al.: The HadGEM2-ES implementation of CMIP5 centennial simulations, Geoscientific Model Development, 4, 543–570, https://doi.org/https://doi.org/10.5194/gmd-4-543-2011, 2011.

Keuler, K., Radtke, K., Kotlarski, S., and Lüthi, D.: Regional climate change over Europe in COSMO-CLM: Influence of emission scenario and driving global model, Meteorologische Zeitschrift, 25, 121–136, https://doi.org/https://doi.org/10.1127/metz/2016/0662, 2016.

Kwak, J., St-Hilaire, A., Chebana, F., and Kim, G.: Summer season water temperature modeling under the climate change: case study for Fourchue River, Quebec, Canada, Water, 9, 346, https://doi.org/10.3390/w9050346, 2017.

Le Moal, M., Gascuel-Odoux, C., Ménesguen, A., Souchon, Y., Étrillard, C., Levain, A., Moatar, F., Pannard, A., Souchu, P., Lefebvre, A., et al.: Eutrophication: A new wine in an old bottle?, Science of the total environment, 651, 1–11, https://doi.org/10.1016/j.scitotenv.2018.09.139, 2019.

Lee, S.-Y., Fullerton, A. H., Sun, N., and Torgersen, C. E.: Projecting spatiotemporally explicit effects of climate change on stream temperature: A model comparison and implications for coldwater fishes, Journal of Hydrology, 588, 125 066, https://doi.org/https://doi.org/10.1016/j.jhydrol.2020.125066, 2020.

Loicq, P., Moatar, F., Jullian, Y., Dugdale, S. J., and Hannah, D. M.: Improving representation of riparian vegetation shading in a regional stream temperature model using LiDAR data, Science of the total environment, 624, 480–490, https://doi.org/10.1016/j.scitotenv.2017.12.129, 2018.

Michel, A., Brauchli, T., Lehning, M., Schaefli, B., and Huwald, H.: Stream temperature and discharge evolution in Switzerland over the last 50 years: annual and seasonal behaviour., Hydrology & Earth System Sciences, 24, https://doi.org/10.5194/hess-24-115-2020, 2020.

Michel, A., Schaefli, B., Wever, N., Zekollari, H., Lehning, M., and Huwald, H.: Future water temperature of rivers in Switzerland under climate change investigated with physics-based models, Hydrology and Earth System Sciences Discussions, pp. 1–45, https://doi.org/https://doi.org/10.5194/hess-2021-194, 2021.

Minaudo, C., Curie, F., Jullian, Y., Gassama, N., and Moatar, F.: QUAL-NET, a high temporal-resolution eutrophication model for large hydrographic networks, Biogeosciences, 15, 2251–2269, https://doi.org/https://doi.org/10.5194/bg-15-2251-2018, 2018.

Moatar, F. and Gailhard, J.: Water temperature behaviour in the River Loire since 1976 and 1881, Comptes Rendus Geoscience, 338, 319–328, https://doi.org/10.1016/j.crte.2006.02.011, 2006.

Morales-Marín, L., Rokaya, P., Sanyal, P., Sereda, J., and Lindenschmidt, K.: Changes in streamflow and water temperature affect fish habitat in the Athabasca River basin in the context of climate change, Ecological Modelling, 407, 108 718, https://doi.org/10.1016/j.ecolmodel.2019.108718, 2019.

410 Nelson, K. C. and Palmer, M. A.: Stream temperature surges under urbanization and climate change: data, models, and responses 1, JAWRA Journal of the American Water Resources Association, 43, 440–452, https://doi.org/10.1111/j.1752-1688.2007.00034.x, 2007.

Orr, H. G., Simpson, G. L., des Clers, S., Watts, G., Hughes, M., Hannaford, J., Dunbar, M. J., Laizé, C. L., Wilby, R. L., Battarbee, R. W., et al.: Detecting changing river temperatures in England and Wales, Hydrological Processes, 29, 752–766, https://doi.org/10.1002/hyp.10181, 2015.

415 Ouellet, V., St-Hilaire, A., Dugdale, S. J., Hannah, D. M., Krause, S., and Proulx-Ouellet, S.: River temperature research and practice: Recent challenges and emerging opportunities for managing thermal habitat conditions in stream ecosystems, Science of the Total Environment, 736, 139 679, https://doi.org/https://doi.org/10.1016/j.scitotenv.2020.139679, 2020.

Picard, C., Floury, M., Seyedhashemi, H., Morel, M., Pella, H., Lamouroux, N., Buisson, L., Moatar, F., and Maire, A.: Direct habitat descriptors improve the understanding of the organization of fish and macroinvertebrate communities across a large catchment, PloS one,

420 17, e0274 167, https://doi.org/https://doi.org/10.1371/journal.pone.0274167, 2022.

Piotrowski, A. P., Osuch, M., and Napiorkowski, J. J.: Influence of the choice of stream temperature model on the projections of water temperature in rivers, Journal of Hydrology, 601, 126 629, https://doi.org/https://doi.org/10.1016/j.jhydrol.2021.126629, 2021.

Quintana-Segui, P., Le Moigne, P., Durand, Y., Martin, E., Habets, F., Baillon, M., Canellas, C., Franchisteguy, L., and Morel, S.: Analysis of near-surface atmospheric variables: Validation of the SAFRAN analysis over France, Journal of applied meteorology and climatology,

425 47, 92–107, https://doi.org/10.1175/2007JAMC1636.1, 2008.

Seixas, G. B., Beechie, T. J., Fogel, C., and Kiffney, P. M.: Historical and Future Stream Temperature Change Predicted by a Lidar-Based Assessment of Riparian Condition and Channel Width, JAWRA Journal of the American Water Resources Association, 54, 974–991, https://doi.org/https://doi.org/10.1111/1752-1688.12655, 2018.

Seyedhashemi, H., Moatar, F., Vidal, J.-P., Diamond, J. S., Beaufort, A., Chandesris, A., and Valette, L.: Thermal signatures iden-

430 tify the influence of dams and ponds on stream temperature at the regional scale, Science of The Total Environment, p. 142667, https://doi.org/10.1016/j.scitotenv.2020.142667, 2020.

Seyedhashemi, H., Moatar, F., Vidal, J.-P., and Thiéry, D.: Past and future discharge and stream temperature at high spatial resolution in a large European basin (Loire basin, France), https://doi.org/10.57745/LBPGFS, 2022a.

Seyedhashemi, H., Vidal, J.-P., Diamond, J. S., Thiéry, D., Monteil, C., Hendrickx, F., Maire, A., and Moatar, F.: Regional, multi-decadal

435 analysis reveals that stream temperature increases faster than air temperature, Hydrology and Earth System Sciences, 26, 2583–2603, https://doi.org/https://doi.org/10.5194/hess-26-2583-2022, 2022b.

Sinokrot, B., Stefan, H., McCormick, J., and Eaton, J.: Modeling of climate change effects on stream temperatures and fish habitats below dams and near groundwater inputs, Climatic Change, 30, 181–200, https://doi.org/10.1007/BF01091841, 1995.

Skamarock, W. C., Klemp, J. B., Dudhia, J., Gill, D. O., Barker, D. M., Wang, W., and Powers, J. G.: A description of the Advanced Research

440 WRF version 3. NCAR Technical note-475+ STR, http://citeseerx.ist.psu.edu/viewdoc/download?doi=10.1.1.484.3656&rep=rep1&type=pdf, 2008.

Soubeyroux, J.-M. et al.: Les nouvelles projections climatiques de référence DRAIS 2020 pour la Métropole, Tech. rep., Météo France, http://www.drias-climat.fr/document/rapport-DRIAS-2020-red3-2.pdf, 2020.

Steel, E. A., Beechie, T. J., Torgersen, C. E., and Fullerton, A. H.: Envisioning, quantifying, and managing thermal regimes on river networks, BioScience, 67, 506–522, https://doi.org/10.1093/biosci/bix047, 2017.

Thiéry, D.: Logiciel ÉROS version 7.1. Guide d'utilisation, in: Rapport BRGM/RP-67704-FR, http://infoterre.brgm.fr/rapports/RP-67704-FR.pdf, 2018.

Thiéry, D. and Moutzopoulos, C.: Un modèle hydrologique spatialisé pour la simulation de très grands bassins: le modèle EROS formé de grappes de modèles globaux élémentaires, VIIIèmes journées hydrologiques de l'ORSTOM" Régionalisation en hydrologie, application au développement", Le Barbé et E. Servat (Eds.), pp. 285–295, https://hal-brgm.archives-ouvertes.fr/hal-01061971, 1995.

van Vliet, M. T., Franssen, W. H., Yearsley, J. R., Ludwig, F., Haddeland, I., Lettenmaier, D. P., and Kabat, P.: Global river discharge and water temperature under climate change, Global Environmental Change, 23, 450–464, https://doi.org/10.1016/j.gloenvcha.2012.11.002, 2013.

Verfaillie, D., Déqué, M., Morin, S., and Lafaysse, M.: The method ADAMONT v1. 0 for statistical adjustment of climate projections applicable to energy balance land surface models, Geoscientific Model Development, 10, 4257–4283, https://doi.org/https://doi.org/10.5194/gmd-10-4257-2017, 2017.

Vidal, J.-P., Martin, E., Franchistéguy, L., Baillon, M., and Soubeyroux, J.-M.: A 50-year high-resolution atmospheric reanalysis over France with the Safran system, International Journal of Climatology, 30, 1627–1644, https://doi.org/10.1002/joc.2003, 2010.

Voldoire, A., Sanchez-Gomez, E., y Mélia, D. S., Decharme, B., Cassou, C., Sénési, S., Valcke, S., Beau, I., Alias, A., Chevallier, M., et al.: The CNRM-CM5. 1 global climate model: description and basic evaluation, Climate dynamics, 40, 2091–2121, https://doi.org/https://doi.org/10.1007/s00382-011-1259-y, 2013.

Wasson, J.-G., Chandesris, A., Pella, H., and Blanc, L.: Typology and reference conditions for surface water bodies in France: the hydro-ecoregion approach, TemaNord, 566, 37–41, https://hal.archives-ouvertes.fr/hal-00475620/document, 2002.

Webb, B. and Walling, D.: Complex summer water temperature behaviour below a UK regulating reservoir, Regulated Rivers: Research & Management: An International Journal Devoted to River Research and Management, 13, 463–477, https://doi.org/10.1002/(SICI)1099-1646(199709/10)13:5<463::AID-RRR470>3.0.CO;2-1, 1997.

Webb, B. W., Hannah, D. M., Moore, D. R., Brown, L. E., and Nobilis, F.: Recent advances in stream and river temperature research, Hydrological Processes: An International Journal, 22, 902–918, https://doi.org/10.1002/hyp.6994, 2008.

Yearsley, J. R.: A semi-Lagrangian water temperature model for advection-dominated river systems, Water Resources Research, 45, https://doi.org/10.1029/2008WR007629, 2009.

Zhao, F., Zhan, X., Xu, H., Zhu, G., Zou, W., Zhu, M., Kang, L., Guo, Y., Zhao, X., Wang, Z., et al.: New insights into eutrophication management: Importance of temperature and water residence time, Journal of Environmental Sciences, 111, 229–239, https://doi.org/https://doi.org/10.1016/j.jes.2021.02.033, 2022.